Top quark anomalous electromagnetic couplings
in photon-photon scattering at the LHC

Sh. Fayazbakhsh,[*] S. Taheri Monfared,[†] and M. Mohammadi Najafabadi[‡]

Institute for Research in Fundamental Sciences (IPM), School of Particles and Accelerators,
P.O. Box 19395-5531 Tehran, Iran

The capability of the LHC to study the electromagnetic dipole moments of the top quark is discussed. In particular, the process $pp \rightarrow p\gamma\gamma p \rightarrow p t\bar{t} p$, which is supposed to be tagged by the forward/backward detectors at the LHC experiments, is used to explore the top quark electric and magnetic moments. We perform analytical calculations and then a numerical analysis on the sensitivity of the total cross section of the top quark pair production in $\gamma\gamma$ scattering at the LHC to the anomalous top quark couplings with photon. It is shown that improvements in the bounds on the electromagnetic dipole moments of the top quark can be achieved in this channel in comparison with the constraints from the former studies.

PACS numbers: 14.65.Ha, 12.60.-i, 14.70.Bh

I. INTRODUCTION

The Standard Model (SM) of particle physics is a well-tested effective theory, applicable at current energies, that precisely illustrates almost all experimental results and a variety of phenomena in particle physics studies, up to now. However, from the phenomenological point of view, one may attempt to model the effects of the electroweak and strong interactions of possible non-SM heavy particles, beyond TeV scale, on the experimental observables at high energy colliders. As a widely accepted framework, the effective Lagrangian approach with the content of several higher-dimension interaction terms has attracted great attention [1–14]. According to the dimensional analysis, such new terms include expansion coefficients which are inversely proportional to powers of Λ, the scale of beyond the SM (BSM) physics.

Among the SM elementary particles, the top quark is the heaviest one, available now, with a mass $m_t \simeq 173.21$ GeV [15] nearly in the same order of the electroweak symmetry breaking energy scale. Therefore, any deviation from the SM results is more traceable in the top quark interactions than the other fermion ones. So far, top quark couplings are not completely investigated and the SM predictions for this heavy fermion have to be tested more in the case where large numbers of top quarks and antiquarks are produced in the LHC.

It is noteworthy that the CP violation in the SM, which is explained with a complex phase in the Cabibbo-Kobayashi-Maskawa matrix, cannot describe the matter-antimatter asymmetry in the universe due to its small amount. This asymmetry is one of the main questions in particle physics that is not answered even in the heavy quarks decay processes.

Thus, the measurement of large amounts of CP violation in the top quark events can be an evidence of BSM physics. Probing the new physics effects, some of the intrinsic properties of the top quark are studied in the context of its dipole moments such as the magnetic dipole moment (MDM) coming from one-loop level perturbations and the corresponding electric dipole moment (EDM), which is described as a source of CP violation [16]. Motivated by the structure of the EDM, achieved from three-loop level perturbations in the SM, one can mutate the top-gauge field vertices through CP-symmetric and CP-asymmetric anomalous form factors in order to explore the non-SM effects in the top quark pair production processes.

In the SM, the top quark EDM is so small that it can be a highly attractive probe of new physics, while the SM prediction for the MDM of this heavy particle is not far from the upcoming experiments [17]. Although EDM and MDM quantities have been long investigated, both theoretically and experimentally, in the case of light quarks, these intrinsic properties still require more improvement on the subject of heavy quark physics. The EDM and MDM values of $\hat{a}_A < 1.75 \times 10^{-14}$ and $\hat{a}_V = 0.013$ are predicted by the SM for top quarks [18,19]. There are numerical analyses based on an extended minimal supersymmetric standard model, including an extra vectorlike multiplet, which predict the top quark EDM close to 1.75×10^{-3} [20]. Indirect measurements, which stand on experimental limits on the neutron EDM, lead to upper bounds of 5.25×10^1 for the top quark EDM [21]. A study on sensitivity of hadron colliders to constrain the top quark dipole moments within $t\bar{t}\gamma$ production has been performed in Ref. [22]. For the LHC at $\sqrt{s} = 14$ TeV, they have reported the limit of ± 0.2 (± 0.1) assuming the integrated luminosity $L_{\text{int}} = 300$ fb^{-1} ($L_{\text{int}} = 3000$ fb^{-1}) of data. More recent limits of $-2.0 \leq \hat{a}_V \leq 0.3$ and $-0.5 \leq \hat{a}_A \leq 1.5$, coming from the branching ratio and a CP asymmetry for $b \rightarrow s\gamma$, is

[*]shfayazbakhsh@ipm.ir
[†]sara.taheri@ipm.ir
[‡]mojtaba@ipm.ir

available in Ref. [23]. The bounds of $|\hat{a}_V| < 0.05(0.09)$ and $|\hat{a}_A| < 0.20(0.28)$ are concluded from potential future measurements of $\gamma e \to t\bar{t}$ cross section with 10% (18%) uncertainty [17]. As will be presented in this paper, our strategy leads to much more stringent limits than the current experimental ones for both EDM and MDM of the top quark.

In this paper, we will focus on the top quark pair production via the central exclusive diffractive production (CEP), which is defined as the process $pp \to p\gamma\gamma p \to pt\bar{t}p$, while there is no radiation between the intact outgoing beam of protons and the central system $t\bar{t}$. In CEP processes, two interacting protons do not dissociate during the collision. In the simplest case, they exchange two photons and survive into the final state with extra centrally produced particle states. These protons are called forward or intact protons. The study of such events, which are classified as the forward physics studies, is becoming popular among some of the ATLAS and CMS collaborations due to the range of exclusive measurements under way at the LHC. Moreover, such collisions experimentally provide a very clean signal and represent a promising way to search for a possible BSM signal in hadron colliders.

Forward protons energies can be described by means of the fractional proton energy loss, $\xi = E_{\text{loss}}/E_p$. Here, E_{loss} is the energy that proton loses in the interaction and E_p is the energy of the incoming proton beam. The ξ parameter represents a region, which is referred to as the forward detector acceptance region, to observe intact protons in the interval $\xi_{\min} < \xi < \xi_{\max}$. Here, based on the CMS and ATLAS standard running conditions, we consider three different classes of the acceptance region to be [24,25]

  (i) $0.0015 < \xi < 0.5$ (CMS-TOTEM),
  (ii) $0.0015 < \xi < 0.15$ (AFP-ATLAS),
  (iii) $0.1 < \xi < 0.5$ (CMS-TOTEM).

Higher ξ is available by installing forward detectors closer to the interaction points. It is worth mentioning that the central exclusive production enables us to probe several physics subjects ranging from the SM tests to searches for new physics such as the anomalous interactions of the gauge bosons and new heavy resonances. Several physics capability searches can be found in [26–47]. In [37], the top quark flavor-changing neutral current in the $tq\gamma$ vertex with $q = u, c$ has been examined using the $pp \to p\gamma\gamma p \to pt\bar{q}p$ process for three acceptance regions of the forward detectors. It is shown that the sensitivity of this channel has the potential to improve the bounds on the branching ratios of $t \to q\gamma$.

The present paper is organized as follows: In Sec. II A, we will introduce an effective Lagrangian for a top quark pair production process that comprises the modified interactions. Thereafter, in Sec. II B, an analytical expression for the total cross section of a diffractive collision at the LHC is provided. To demonstrate the effect of anomalous couplings on the top quark pair production process, Sec. III is

devoted to a complete numerical analysis on the coupling constant dependence of the total cross section as well as the backgrounds to the equivalent photon approximation (EPA) method. The constraints on the BSM couplings values are also discussed. In Sec. IV our concluding remarks are presented.

II. THEORETICAL ANALYSIS

A. The top quark effective electromagnetic interactions

To clarify our framework we start with a model independent approach which relies on a low energy effective field theory. In the effective field theory approach, effective interactions among only the SM particles are obtained by integrating out the high scale physics. The effective interactions are suppressed by the inverse powers of Λ which is defined as the scale at which the new physics effects appear. The SM is the low energy limit of the effective theory which has to satisfy the symmetry of $SU(3) \times SU(2) \times U(1)$. Neglecting the possible dimension five operator which breaks the lepton number conservation [48], the leading effects can be parametrized by dimension six operators:

$$\mathcal{L}_{\text{eff}} = \mathcal{L}_{\text{SM}} + \sum_i \frac{c_i O_i}{\Lambda^2} + \text{H.c.}, \tag{2.1}$$

where the dimension six operators are denoted by O_i and c_i are dimensionless coefficients. The dimension six operators involving top quark affect Wtb, Ztt, γtt, and gtt vertices which are presented in [12] and references therein. After including the contributions of dimension six operators, the γtt vertex takes the following form[1] [12]:

$$\mathcal{L}_{\text{eff}} = -g_e Q_t \bar{\psi}_t \left(\gamma^\mu + \frac{i}{2m_t}(\hat{a}_V + i\hat{a}_A\gamma^5)\sigma^{\mu\nu}k_\nu \right)\psi_t A_\mu. \tag{2.2}$$

Here, A_μ and Q_t are the photon gauge field and the top quark electric charge, respectively. The top quark field, ψ_t, belongs to the fundamental representation of the $SU(3)_c$ color group and g_e is the electromagnetic coupling constant. The non-SM couplings are denoted by real parameters $\hat{a}_V$ and $\hat{a}_A$, which indicate the top quark magnetic and electric dimensionless dipole moments, respectively. Hence, these quantities are proportional to the corresponding quark anomalous dipole moments. Here, k_ν defines the photon four-momentum and $m_t \simeq 173.21$ GeV is the top quark mass. The term $\gamma^5\sigma^{\mu\nu}$, with $\sigma^{\mu\nu} = i[\gamma^\mu, \gamma^\nu]/2$, breaks the CP symmetry, so the coefficient $\hat{a}_A$ determines the strength of a possible CP violation process, which might originate from new physics.

---

[1]The modifications of the γtt vertex particularly arise from dimension six operators of O_{uW} and $O_{uB\phi}$ in the notation of Ref. [12].

B. Theoretical calculations

A representative Feynman diagram for the two-photon CEP process $pp \rightarrow p\gamma\gamma p \rightarrow pt\bar{t}p$ is illustrated in Fig. 1. Here, two quasielastically incoming protons fluctuate two photons. The emitted photons can collide and produce a pair of top quarks which can be observed in the central detectors. The scattering amplitudes for on-mass-shell photons, using the relation $\hat{s} = 2m_t^2 - \hat{t} - \hat{u}$ and the redefinition $R_{AV}^2 = \hat{a}_A^2 + \hat{a}_V^2$, read

$$
\begin{aligned}
|M_1|^2 = \frac{8\pi^2\alpha_e^2 Q_t^2}{(m_t^2 - \hat{t})^2} \{ & m_t^4[(R_{AV}^2 + 12\hat{a}_V)^2 + 50R_{AV}^2 - 72(\hat{a}_V - 1)^2 + 56] \\
& - m_t^2[(3\hat{t} + \hat{u})(R_{AV}^2 + 6\hat{a}_V + 4)^2 + 6\hat{t}(R_{AV}^2(17 + 4\hat{a}_V) + 16\hat{a}_V)] \\
& + 3\hat{t}^2[(R_{AV}^2 + 8\hat{a}_V)^2 + 34R_{AV}^2 - 52\hat{a}_V^2 + 32\hat{a}_V] \\
& + \hat{t}\,\hat{u}[3(R_{AV}^2 + 4\hat{a}_V)^2 - 12(\hat{a}_V - 2)^2 + 16(R_{AV}^2 + 4)]\},
\end{aligned}
\tag{2.3}
$$

$$
\begin{aligned}
|M_2|^2 = \frac{8\pi^2\alpha_e^2 Q_t^2}{(m_t^2 - \hat{u})^2} \{ & m_t^4[(R_{AV}^2 + 12\hat{a}_V)^2 + 50R_{AV}^2 - 72(\hat{a}_V - 1)^2 + 56] \\
& - m_t^2[(\hat{t} + 3\hat{u})(R_{AV}^2 + 6\hat{a}_V + 4)^2 + 6\hat{u}(R_{AV}^2(17 + 4\hat{a}_V) + 16\hat{a}_V)] \\
& + 3\hat{u}^2[(R_{AV}^2 + 8\hat{a}_V)^2 + 34R_{AV}^2 - 52\hat{a}_V^2 + 32\hat{a}_V] \\
& + \hat{t}\,\hat{u}[3(R_{AV}^2 + 4\hat{a}_V)^2 - 12(\hat{a}_V - 2)^2 + 16(R_{AV}^2 + 4)]\},
\end{aligned}
\tag{2.4}
$$

$$
\begin{aligned}
M_1 M_2^* + M_2 M_1^* = \frac{16\pi^2\alpha_e^2 Q_t^2}{(m_t^2 - \hat{t})(m_t^2 - \hat{u})} \{ & -2m_t^4[R_{AV}^2(2R_{AV}^2 + 12\hat{a}_V + 17) + 20(\hat{a}_V + 1)^2 - 4] \\
& + m_t^2(\hat{t} + \hat{u})[2(R_{AV}^2 + 5\hat{a}_V)^2 + 35(R_{AV}^2 - \hat{a}_V)^2 + (5\hat{a}_V + 8)^2 - 80] \\
& - (\hat{t}^2 + \hat{u}^2)[R_{AV}^2(4\hat{a}_V + 5) + 10\hat{a}_V^2 + 8\hat{a}_V] + 4\hat{t}\,\hat{u}[R_{AV}^2(R_{AV}^2 - 7) - 5\hat{a}_V^2 - 16\hat{a}_V]\},
\end{aligned}
\tag{2.5}
$$

where, $\hat{s} = (p_1 + p_2)^2 = (k_1 + k_2)^2$, $\hat{t} = (p_1 - k_1)^2 = (k_2 - p_2)^2$, $\hat{u} = (k_1 - p_2)^2 = (p_1 - k_2)^2$ and p_i (k_i) with $i = 1, 2$ is the four-momentum of the final top quark (the initial photon).

Before going any further with computing the total cross section we have to simplify the whole process making use of the EPA. As a proper theoretical tool, the EPA method can be applied to processes of the type $AB \rightarrow A\gamma^*B \rightarrow AX$, which involve virtual photons fusion. If γ^* can be treated as an almost real photon, such an approximation suggests that one can reduce the cross section of $AB \rightarrow AX$ to that of the subprocess $\gamma^*B \rightarrow X$. In a typical scattering process of a quark from a proton the corresponding amplitude is seriously sizable in the forward direction where the exchanged photon momentum is almost zero. Consequently, in this limit, the virtual photon turns into a quasireal photon and the EPA is justified to describe the photon spectrum in terms of its virtuality, Q^2, and energy, E_γ, as
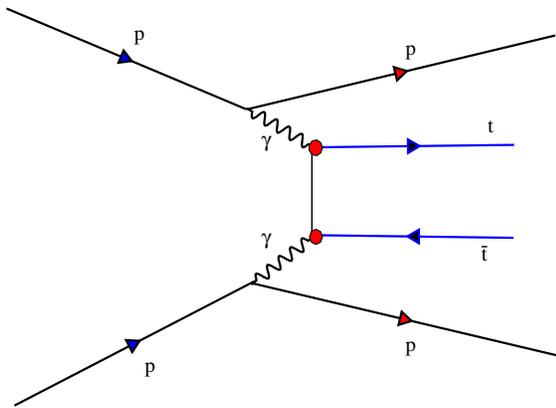

FIG. 1 (color online). A schematic Feynman diagram for the two-photon exclusive top quark pair production process $pp \rightarrow p\gamma\gamma p \rightarrow pt\bar{t}p$.

$$
\begin{aligned}
f(E_\gamma, Q^2) = \frac{dN}{dE_\gamma dQ^2} = \frac{\alpha_e}{\pi} \frac{1}{E_\gamma Q^2} \\
\times \left[\left(1 - \frac{E_\gamma}{E_p}\right)\left(1 - \frac{Q_{\min}^2}{Q^2}\right)F_E + \frac{E_\gamma^2}{2E_p^2}F_M \right].
\end{aligned}
\tag{2.6}
$$

In what follows, we use the relation $E_\gamma = E_p \xi$ and in the dipole approximation the definitions

$$Q^2_{\min} = \frac{E_\gamma^2 m_p^2}{E_p(E_p - E_\gamma)},$$

$$F_E = \frac{4m_p^2 G_E^2 + Q^2 G_M^2}{4m_p^2 + Q^2}, \qquad F_M = G_M^2,$$

$$G_E^2 = \frac{G_M^2}{\mu_p^2} = \left(1 + \frac{Q^2}{Q_0^2}\right)^{-4}, \qquad Q_0^2 = 0.71 \text{ GeV}^2,$$

(2.7)

are employed [49–52] where $\alpha_e = g_e^2/4\pi$ is the fine-structure constant, m_p is the proton mass, and the squared magnetic moment of the proton is taken to be a constant value $\mu_p^2 = 7.78$. Here, F_M and F_E are relative to the proton magnetic and electric form factors, respectively.

In a general CEP process, the invariant mass of centrally produced particles, with energies E_1 and E_2, is obtained from $\omega \simeq 2\sqrt{E_1 E_2}$. Within such events at the LHC, the invariant mass can extend to the scales which are high enough to be explored for possible new physics. In our CEP process, Fig. 1, the produced particles are two quasireal photons with $\omega \simeq 2\sqrt{E_{\gamma_1} E_{\gamma_2}}$. Thus, the luminosity spectrum of the emitted photons can be introduced by integrating the product of two photon spectra over the photon virtualities and energies, keeping ω fixed. Evaluating the integration by changing variables from energies of two photons to y and $\omega^2/4y$, where the photon virtualities remain unchanged, we arrive at the $\gamma\gamma$ luminosity spectrum

$$\frac{dL^{\gamma\gamma}}{d\omega} = \int_{y_{\min}}^{y_{\max}} \frac{\omega}{2y} dy \int_{Q^2_{1,\min}}^{Q^2_{\max}} dQ_1^2 \int_{Q^2_{2,\min}}^{Q^2_{\max}} dQ_2^2 f\left(\frac{\omega^2}{4y}, Q_1^2\right) f(y, Q_2^2). \tag{2.8}$$

Virtuality of colliding photons varies between the kinematical minimum, $Q^2_{\min}$, and a maximum, $Q^2_{\max} \sim 1/R^2$, where R is the proton radius [50,52]. We can conclude, from relations (2.7), that the electric and magnetic proton form factors fall rapidly with the increase of Q^2. Hence, the contribution of higher virtualities, more than $Q^2_{\max} = 2$ GeV^2, to the integral (2.8) is negligible.

The total cross section that is derived by integrating $\hat{\sigma}_{\gamma\gamma \to t\bar{t}}$, the cross section of the selected subprocess, is as follows [53]:

$$\sigma = \int_{\omega_{\min}}^{\omega_{\max}} d\omega \int_{y_{\min}}^{y_{\max}} \frac{\omega}{2y} dy \int_{Q^2_{1,\min}}^{Q^2_{\max}} dQ_1^2 \int_{Q^2_{2,\min}}^{Q^2_{\max}} dQ_2^2 f\left(\frac{\omega^2}{4y}, Q_1^2\right) f(y, Q_2^2) \hat{\sigma}_{\gamma\gamma \to t\bar{t}}(Q_1^2, Q_2^2, y, \omega). \tag{2.9}$$

In this formalism photons are supposed to be off-shell particles in order to produce top quark pairs, so $\hat{\sigma}_{\gamma\gamma \to t\bar{t}}$ in relation (2.9) also depends on photons virtualities and energies.

III. NUMERICAL ANALYSIS

A. The cross section dependence on top quark anomalous couplings

In this section, we make a numerical analysis on the anomalous electromagnetic couplings and extract the allowed regions of these parameters. At the first step, the behavior of the $\gamma\gamma$ luminosity spectrum as a function of ω at $\sqrt{s} = 14$ TeV and for the region $0.0015 < \xi < 0.5$ is shown in Fig. 2. The numerical calculations are performed with the integration limits

$$y_{\min} = \text{Max}\left[\frac{\omega^2}{4E_p \xi_{\max}}, E_p \xi_{\min}\right],$$

$$y_{\max} = \text{Min}\left[\frac{\omega^2}{4E_p \xi_{\min}}, E_p \xi_{\max}\right],$$

$$\omega_{\min} = \text{Max}[2m_t, 2E_p \xi_{\min}], \qquad \omega_{\max} = \sqrt{s}, \tag{3.1}$$

which are determined in terms of two boundaries of the acceptance region, $\xi_{\min}$ and $\xi_{\max}$. Moreover, one may use the relation $y_{\max} = E_p \xi_{\max}$ instead of the one in (3.1) and no noticeable difference appears.

In Figs. 3 and 4 the dependency of the total cross section to the top quark EDM and MDM is studied at the center of mass energies $\sqrt{s} = 14$ and $\sqrt{s} = 33$ TeV, respectively. This type of dependence is illustrated for three different
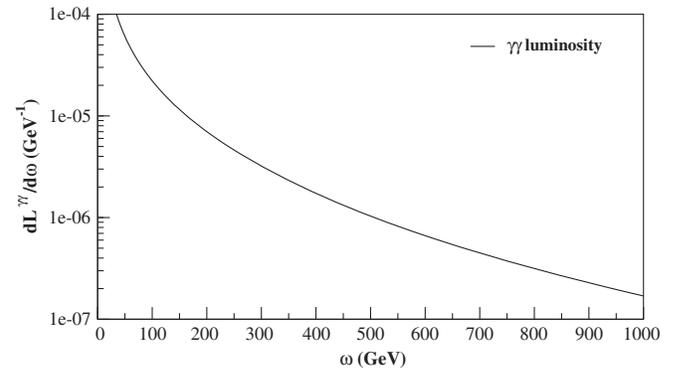

FIG. 2. Photon luminosity as a function of ω at $\sqrt{s} = 14$ TeV and for the acceptance region $0.0015 < \xi < 0.5$.
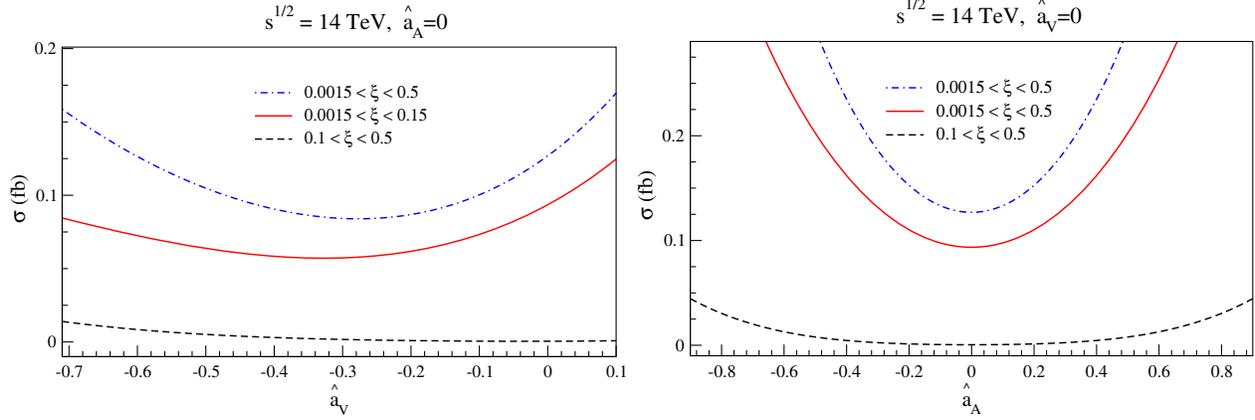
FIG. 3 (color online).   The total cross section of the process $p\gamma\gamma p \to p t\bar{t} p$ as a function of the anomalous coupling $\hat{a}_V$ at $\hat{a}_A = 0$ (left panel) and $\hat{a}_A$ at $\hat{a}_V = 0$ (right panel), at center of mass energy $\sqrt{s} = 14$ TeV. The curves show the sensitivity for three different acceptance regions remarked on the figure.
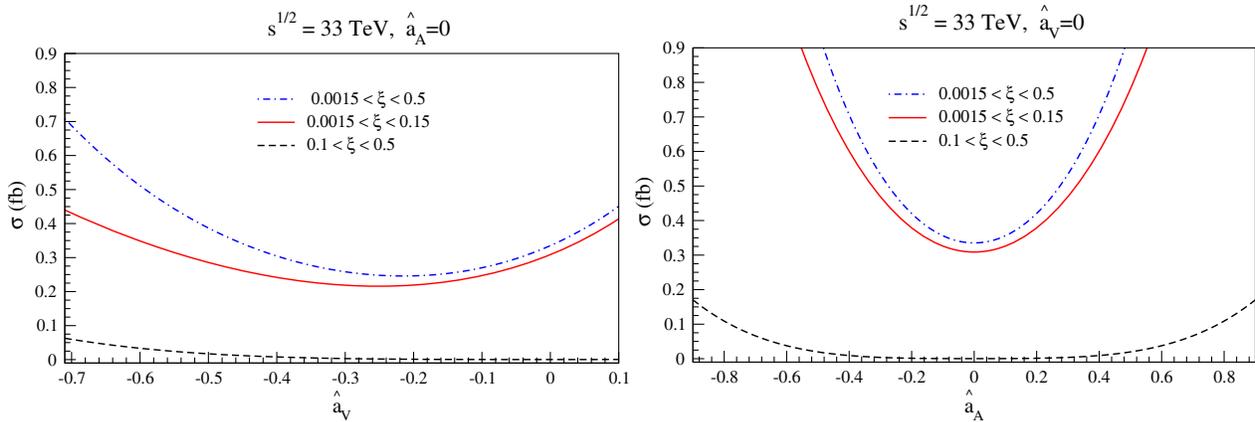

FIG. 4 (color online).   The total cross section of the process $p\gamma\gamma p \to p t\bar{t} p$ as a function of the anomalous coupling $\hat{a}_V$ at $\hat{a}_A = 0$ (left panel) and $\hat{a}_A$ at $\hat{a}_V = 0$ (right panel), at center of mass energy $\sqrt{s} = 33$ TeV. The curves show the sensitivity for three different acceptance regions remarked on the figure.

acceptance detector regions by three separated curves. In each figure, the left (right) panel shows the sensitivity of the cross section to the magnetic (electric) form factor, whereas the electric (magnetic) anomalous coupling is kept fixed at zero.

The first acceptance region of $0.0015 < \xi < 0.5$ provides the most sensitive interval to the anomalous couplings. As it turns out, there is no significant difference between the results of the second region, $0.0015 < \xi < 0.15$, and those of the first one due to almost close cross sections. This means that the upper boundary of the acceptance region does not play indeed a major role in the total cross section value. Comparing the curves in Figs. 3 and 4, we see that the sensitivity increases with increasing center of mass energy.

It is analytically traceable that $\hat{\sigma}_{\gamma\gamma \to t\bar{t}}$ is an even function of $\hat{a}_A$ and a nonzero value of the EDM parameter

always has a constructive effect on the total cross section.[2] By contrast, in the left panel curves, there are small intervals in the vicinity of $\hat{a}_V = 0$ in which the non-SM cross section is smaller than the SM one and as a result the MDM parameter has a partly destructive effect on the top quark pair production process. In each destructive interval there is a global minimum point, $\hat{a}_{V,m}$, that makes the difference $\delta\sigma(\hat{a}_A = 0, \hat{a}_V) = |\sigma_{SM}(pp \to p t\bar{t} p) - \sigma(\hat{a}_A = 0, \hat{a}_V)|$ maximum.[3] In Table I, the values of minima together with the corresponding cross sections, σ_{Min}

---

[2]The γ_5 matrix in the EDM term of Eq. (2.2) breaks the *CP* symmetry and it also prevents the odd powers of $\hat{a}_A$ in the scattering amplitude.

[3]To simplify our notations, from now on in this paper, we will ignore the argument in the SM cross section and indicate it by $\sigma_{SM}(pp \to p t\bar{t} p) = \sigma(\hat{a}_A = 0, \hat{a}_V = 0)$.

TABLE I.   The $\hat{a}_{V,m}$ values together with the maximum deviation of the corresponding cross sections for three forward detector acceptance regions at $\sqrt{s} = 14$ TeV and $\hat{a}_A = 0$.

ξ	$\hat{a}_{V,m}$	σ_{SM} (fb)	$\sigma_{Min}(\hat{a}_{V,m})$ (fb)	$\delta\sigma(\hat{a}_{V,m})$ (fb)	$\delta\sigma(\hat{a}_{V,m})/\sigma_{SM}$
0.0015–0.5	−0.28	0.126892	0.083981	0.042910	0.338
0.0015–0.15	−0.33	0.093597	0.057134	0.057134	0.390
0.1–0.5	−0.04	0.000487	0.000469	0.000018	0.037

$(\hat{a}_A = 0, \hat{a}_{V,m})$, at $\sqrt{s} = 14$ TeV are presented for three acceptance regions. As an example, the maximum deviation of the cross section in the second region occurs at $\hat{a}_{V,m} = -0.33$, which leads to the ratio of $\delta\sigma(\hat{a}_A = 0, \hat{a}_{V,m})/\sigma_{SM}(pp \to p t\bar{t} p) = 0.39$. In other words the possible new physics can be observed if the LHC detectors would be able to measure the cross section of the diffractive top quark pair production with a precision better than 39%. During a typical production process, new physics signatures may not necessarily induce an excess in the cross section rate but in some rare cases a suppression in the normal expected SM rates can also be an evidence of non-SM effects. In the case of our current paper, this fact is confirmed by the destructive behavior of the anomalous MDM parameter in a small interval around $\hat{a}_V = 0$.

B. Constraints on top quark anomalous couplings

In order to obtain constraints on the top quark dipole moments, $(\hat{a}_A, \hat{a}_V)$, a counting experiment is used. The procedure is to start with a Poisson distribution as the probability of measuring n events:

$$P(n|\sigma_{signal}\varepsilon L_{int}\mathrm{Br}, b) = e^{-(b+\sigma_{signal}\varepsilon L_{int}\mathrm{Br})}\frac{(b+\sigma_{signal}\varepsilon L_{int}\mathrm{Br})^n}{n!},$$
(3.2)

where, σ_{signal}, ε, L_{int}, Br, and b are the cross section of the signal in the presence of the anomalous couplings, the

efficiency of the signal, the integrated luminosity, the branching ratio of the process, and the expected number of background events. In the current paper, we only consider the main irreducible background, i.e., the SM process $pp \to p t\bar{t} p$. There could be negligible background contributions from the processes with no top quark in the final state which are not considered in this analysis. This type of backgrounds can be significantly suppressed by applying proper cuts and requirements that must be done by the experimental collaborations. At confidence level of 68%, an upper limit on the signal cross section, σ_{signal}, is calculated by integrating over the posterior probability as follows:

$$0.68 = \frac{\int_0^{\sigma^{68\%}} P(n|\sigma_{signal}\varepsilon L_{int}\mathrm{Br}, b)}{\int_0^\infty P(n|\sigma_{signal}\varepsilon L_{int}\mathrm{Br}, b)}.$$
(3.3)

Here, b denotes the number of expected events without anomalous couplings which is derived from $b = \varepsilon \times L_{int} \times \mathrm{Br} \times \sigma_{bkg}$. The term σ_{bkg} is the background cross section, i.e., $pp \to p t\bar{t} p$ in the SM framework.

To extract the expected limit on the signal cross section, one has to solve Eq. (3.3) by setting the inputs for the number of expected background events and the signal efficiency for a given integrated luminosity and branching ratio. The top quark almost always decays into a W boson and a b-quark. The decays are topologically characterized by the decay of the W boson, either leptonically $[\mathrm{Br}(W \to l\nu) = 0.33]$, or hadronically $[\mathrm{Br}(W \to q\bar{q}) = 0.67]$. We consider the events that one of the top quarks decays

TABLE II.   Sensitivity of the process $pp \to p\gamma\gamma p \to p t\bar{t} p$ to the top quark EDM and MDM achievable at 68% C.L. for $\sqrt{s} = 14, 33$ TeV, integrated luminosities $L_{int} = 100, 300, 3000$ fb^{-1}, and three intervals of forward detector acceptance ξ. The efficiency ε is taken to be 0.9 and $\sigma_{bkg} = \sigma_{SM}(pp \to p t\bar{t} p)$.

| ξ	L_{int} (fb^{-1})	$\hat{a}_V$ $\sqrt{s} = 14$ TeV	$|\hat{a}_A|$ $\sqrt{s} = 14$ TeV	$\hat{a}_V$ $\sqrt{s} = 33$ TeV	$|\hat{a}_A|$ $\sqrt{s} = 33$ TeV
	100	−0.754, 0.105	0.266	−0.524, 0.079	0.192
0.0015–0.5	300	−0.691, 0.067	0.202	−0.489, 0.048	0.148
	3000	−0.639, 0.023	0.116	−0.459, 0.017	0.082
	100	−1.053, 0.123	0.308	−0.649, 0.079	0.206
0.0015–0.15	300	−0.945, 0.078	0.226	−0.615, 0.054	0.154
	3000	−0.837, 0.028	0.134	−0.541, 0.016	0.090
	100	−0.416, 0.301	0.347	−0.235, 0.207	0.224
0.1–0.5	300	−0.338, 0.233	0.277	−0.192, 0.166	0.180
	3000	−0.213, 0.132	0.164	−0.122, 0.104	0.110
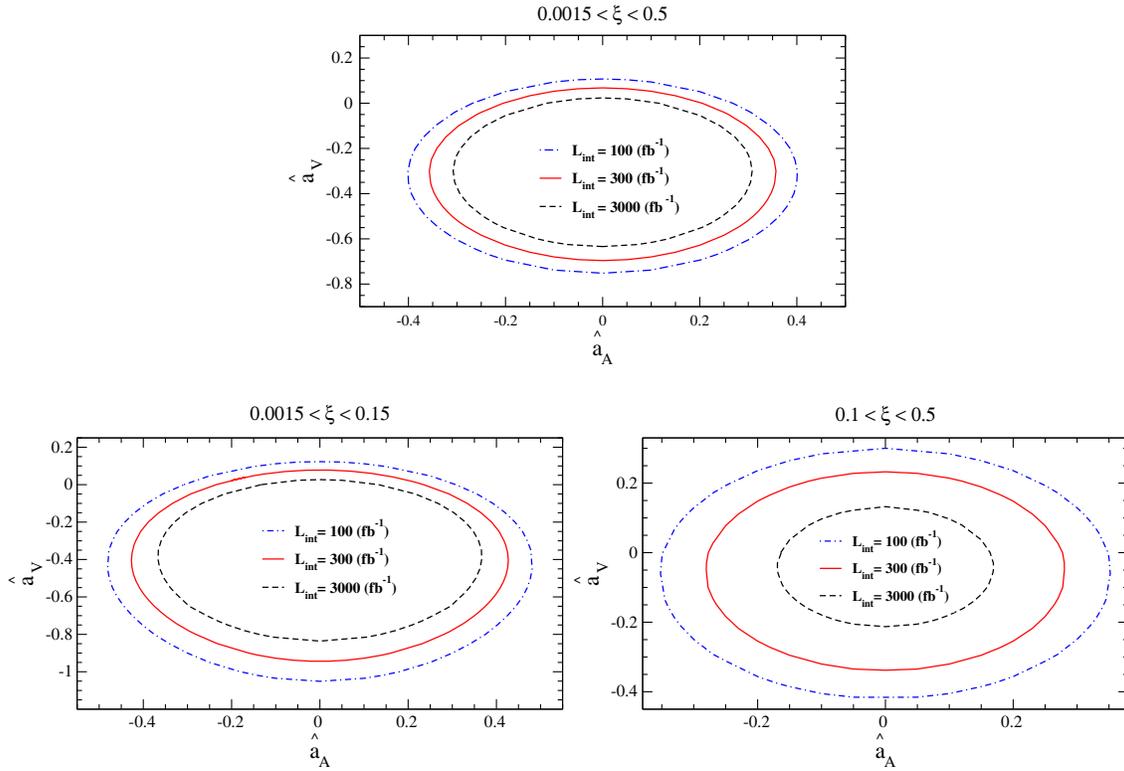
FIG. 5 (color online). The contour diagram in $\hat{a}_V - \hat{a}_A$ plane with 68% C.L. and $\sigma_{\text{bkg}} = \sigma_{\text{SM}}(pp \to pt\bar{t}p)$ at $\sqrt{s} = 14$ TeV, $\varepsilon = 0.9$, and $L_{\text{int}} = 100, 300, 3000$ fb^{-1}. The diagrams are plotted for three different acceptance regions.

leptonically and the other one decays either leptonically or hadronically (so-called semileptonic and dileptonic top quark pair events). Simultaneous hadronic decays of both top quarks is ignored to avoid large background events from the QCD production. Thus, the semileptonic and dileptonic branching ratios are taken into account and the final state joint branching ratio is Br = 0.543 [15].

The efficiency, ε, is the survival probability factor which is important for the predictions and it depends on the detector performance. This factor gives indeed the probability for the absence of extra inelastic interactions beside

diffractive events. To obtain the efficiency, a real experimental simulation has to be done which is beyond the scope of the current paper. Although for central diphoton exchange in $\gamma\gamma$ collision ε is considered to be 0.9 [29,54], in the following we extend our analysis to three different efficiency values, $\varepsilon = 0.1, 0.5, 0.9$.

Table II represents the constraints on the anomalous couplings of top quarks at $\sqrt{s} = 14, 33$ TeV for three different forward detector acceptance regions and integrated luminosities, $L_{\text{int}} = 100, 300, 3000$ fb^{-1}, assuming an optimistic value for the efficiency, $\varepsilon = 0.9$, and the
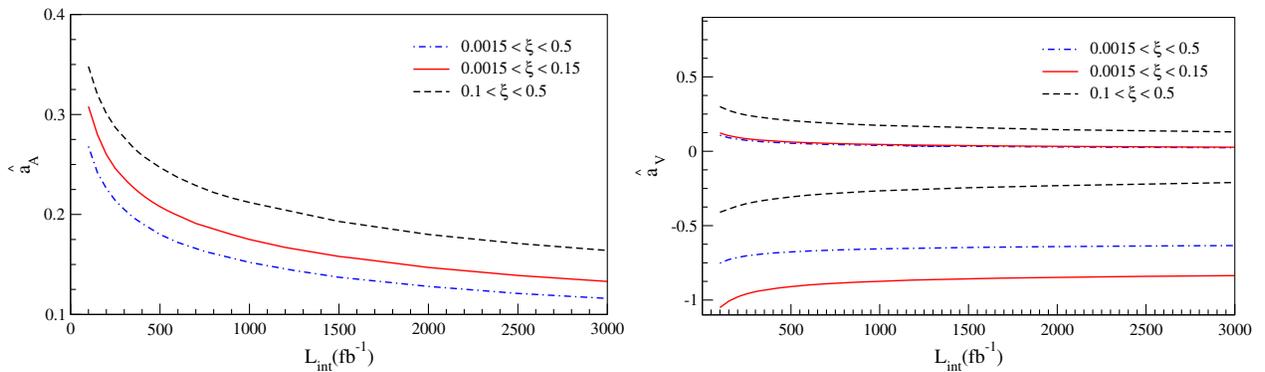

FIG. 6 (color online). The anomalous coupling $\hat{a}_A$ at $\hat{a}_V = 0$ (left panel) and $\hat{a}_V$ at $\hat{a}_V = 0$ (right panel) as a function of integrated luminosity, at $\sqrt{s} = 14$ TeV, $\varepsilon = 0.9$, and $\sigma_{\text{bkg}} = \sigma_{\text{SM}}(pp \to pt\bar{t}p)$ and with 68% C.L. The curves show the sensitivity for three different acceptance regions.

TABLE III.   The Numerical coefficients in the power expansion of total cross section in Eq. (3.4).

ξ	α (fb)	γ (fb)	β (fb)	ρ (fb)	η (fb)	α' (fb)	β' (fb)	δ (fb)	δ' (fb)
0.0015–0.5	0.255	0.549	0.805	0.341	0.127	0.255	0.635	0.510	0.549
0.0015–0.15	0.0953	0.349	0.539	0.254	0.0936	0.0953	0.412	0.191	0.349
0.1–0.5	0.0443	0.0182	0.0191	0.0012	0.00049	0.0443	0.0185	0.0886	0.0182

background cross section $\sigma_{\text{bkg.}} = \sigma_{\text{SM}}(pp \to pt\bar{t}p)$. The first (third) acceptance region, $0.0015 < \xi < 0.5$ ($0.1 < \xi < 0.5$), is the most sensitive interval to $\hat{a}_A$ ($\hat{a}_V$). Increasing the center of mass energy as well as the integrated luminosity provide more restricted bounds on both the anomalous couplings in all the ξ values.

The contour diagrams for the constraints on the anomalous couplings in the $\hat{a}_V - \hat{a}_A$ plane are plotted in Fig. 5, at three different integrated luminosities $L_{\text{int}} = 100, 300, 3000$ fb^{-1} with 68% C.L. Similar to the analysis in Table II, the efficiency and the background cross section are set to be $\varepsilon = 0.9$ and $\sigma_{\text{bkg}} = \sigma_{\text{SM}}(pp \to pt\bar{t}p)$, respectively. Each panel contains the results of a specific acceptance region and, as before mentioned, there is a minor difference between the curves of the first and the second regions in which the lower boundaries are the same.

In Fig. 6, left panel (right panel), the behavior of the limit on the anomalous coupling $\hat{a}_A$ ($\hat{a}_V$) at 68% C.L. as a function of integrated luminosity, at center of mass energy

$\sqrt{s} = 14$ TeV, $\varepsilon = 0.9$, and $\sigma_{\text{bkg}} = \sigma_{\text{SM}}(pp \to pt\bar{t}p)$ is depicted. To extract the above bounds on $\hat{a}_V$ and $\hat{a}_A$, we consider the SM top quark pair production of $pp \to p\gamma\gamma p \to pt\bar{t}p$ as the background and assume the efficiency of observing signal and background events to be $\varepsilon = 0.9$. The curves are presented for three different forward detector acceptance regions. As it can be seen, the 68% C.L. sensitivity on the top quark EDM is more than its MDM to the amount of data. This is because of the stronger dependence of the signal cross section on $\hat{a}_A$ than $\hat{a}_V$. The most sensitive region to the $\hat{a}_A$ ($\hat{a}_V$) parameter is the first (third) acceptance interval.

To have a detailed study on the cross section behavior, we present the analytical form of our theoretical cross section in terms of the anomalous couplings,

$$\sigma(\hat{a}_A, \hat{a}_V) = \alpha\hat{a}_V^4 + \gamma\hat{a}_V^3 + \beta\hat{a}_V^2 + \rho\hat{a}_V + \eta + \alpha'\hat{a}_A^4$$
$$+ \beta'\hat{a}_A^2 + \delta\hat{a}_A^2\hat{a}_V^2 + \delta'\hat{a}_A^2\hat{a}_V. \qquad (3.4)$$
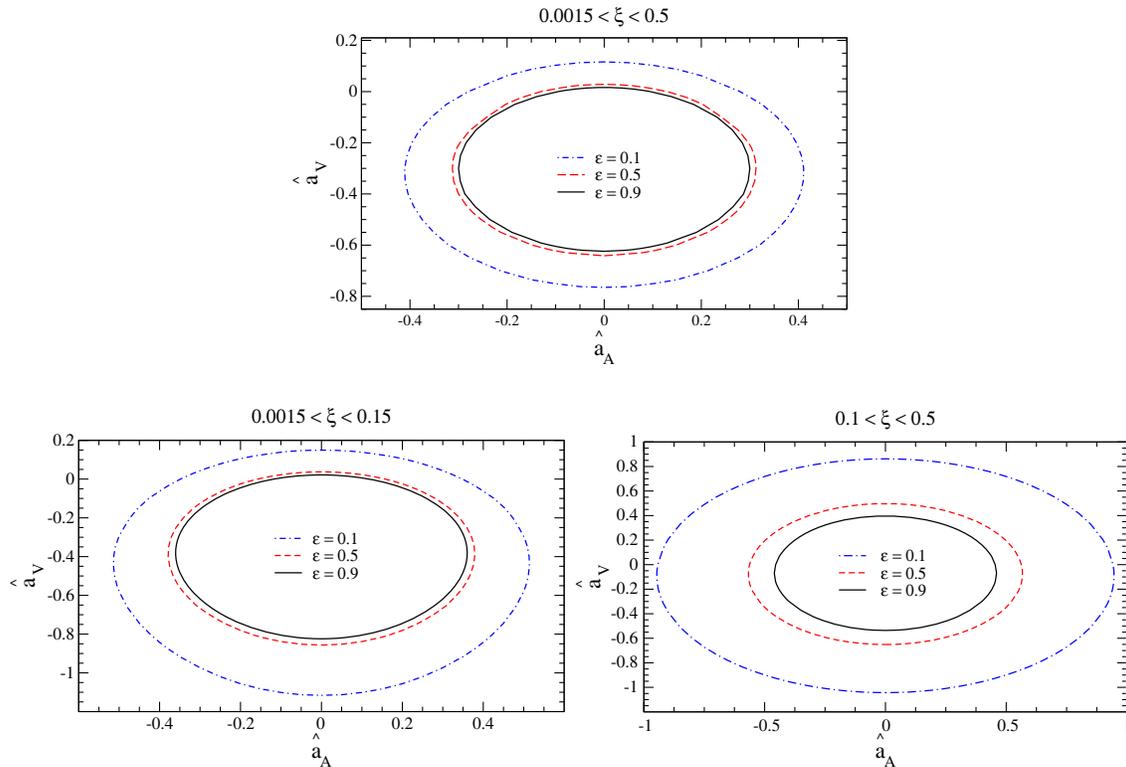

FIG. 7 (color online).   The contour diagram in the $\hat{a}_V - \hat{a}_A$ plane with 68% C.L. at $\sqrt{s} = 14$ TeV, $L_{\text{int}} = 3000$ fb^{-1}, and $\varepsilon = 0.1, 0.5, 0.9$. Total background has been taken 10 times more than signal. The diagrams are plotted for three different acceptance regions.

The expansion coefficients, arising from the structure of the scattering amplitudes in (2.3)–(2.5), are summarized in Table III. The parameter η is the cross section at $\hat{a}_A = \hat{a}_V = 0$ that represents the SM cross section magnitude. It is notable that the coefficient of $\hat{a}_A^2 \hat{a}_V^2$, δ, is the sum of the $\hat{a}_A^4$ and $\hat{a}_V^4$ coefficients, i.e., $\delta = \alpha + \alpha'$, also $\delta' = \gamma$. According to Eq. (3.4) and Fig. 3, the bounds on anomalous couplings receive unequal contributions from two different features of the total cross section: the number of contributing background events, $\sigma_{\text{SM}}(pp \to pt\bar{t}p)$, and the slope of its changes with respect to $\hat{a}_A$ and $\hat{a}_V$. It is the latter quantity that plays the main role on the bounds sensitivity in such a way that the existence of different slopes on two sides of the vertical axes in Fig. 3, leads to different upper and lower bounds on EDM and MDM.

To check the dependency of limits to the efficiency and to be more conservative on the background contributions, we get the limits on $\hat{a}_A$ and $\hat{a}_V$ for three efficiency values of 0.1, 0.5, and 0.9 under the assumption that the number of background is 10 times more than that of the signal. The effect of the efficiency reduction and the conservative assumption for background contributions on the bounds of $\hat{a}_A$ and $\hat{a}_V$ at 68% C.L. is illustrated in Fig. 7. The results are presented for three forward detector acceptance regions and integrated luminosity $L_{\text{int}} = 3000$ fb^{-1}.

As it was expected, the limits get looser with respect to the previous shown results in Table II, due to the smaller number of signal events and larger background contributions. Comparing the results of the optimal first detector acceptance region in Fig. 7 with the corresponding data in Fig. 5 at $L_{\text{int}} = 3000$ fb^{-1}, one can conclude that increasing the amount of background by a factor of 10 leads to looser bounds by a factor of around 2–3. Decreasing the efficiency from 0.9 to 0.5 does not significantly affect the limits while going down to 0.1 non-negligibly loosens the bounds on the electromagnetic moments of the top quark. Even in such a pessimistic case, the limits are comparable with the ones from other studies mentioned in the first section.

IV. CONCLUDING REMARKS

The LHC is going to collide proton beams and get data for its second run. It allows one to study a new energy and luminosity beyond the capabilities of the previous particle colliders. In addition to a proton-proton collider, the LHC can be considered as a photon-photon collider where not only the SM could be examined but also several physics beyond the SM could be tested with small backgrounds and a clean environment due to the absence of proton beam remnants. The $\gamma\gamma$ fusion enables us to probe in particular the electromagnetic properties of the SM particles.

In this paper, we have explored the phenomenology of anomalous $\gamma t\bar{t}$ couplings in the subprocess $\gamma\gamma \to t\bar{t}$ in pp collisions at the center of mass energies $\sqrt{s} = 14, 33$ TeV and integrated luminosities $L_{\text{int}} = 100, 300, 3000$ fb^{-1}. We calculate the cross section of the process $pp \to p\gamma\gamma p \to pt\bar{t}p$ for three different detector acceptance regions, $0.0015 < \xi < 0.5$, $0.0015 < \xi < 0.15$, and $0.1 < \xi < 0.5$. We have found more sensitivity to the top quark EDM with respect to the MDM in this process. The detector acceptance region of $0.0015 < \xi < 0.5$ provides stronger bounds. The 68% C.L. bounds on the top quark electric and magnetic dipole moments at the LHC with the center of mass energy of 14 TeV are found to be in the intervals of $(-0.116, 0.116)$ and $(-0.639, 0.023)$ using $L_{\text{int}} = 3000$ fb^{-1} of data, respectively. Finally, it should be mentioned that to obtain more realistic bounds on the anomalous $\gamma t\bar{t}$ couplings, all sources of backgrounds as well as detector effects have to be considered by the experimental collaborations.

[1] B. Henning, X. Lu, and H. Murayama, How to use the Standard Model effective field theory, arXiv:1412.1837.

[2] J. Gonzalez-Fraile, Effective Lagrangian approach to the EWSB sector, arXiv:1411.5364.

[3] L. Lehman, Extending the standard model effective field theory with the complete set of dimension-7 operators, Phys. Rev. D **90**, 125023 (2014).

[4] C. Englert and M. Spannowsky, Effective theories and measurements at colliders, Phys. Lett. B **740**, 8 (2015).

[5] E. Masso, An effective guide to beyond the Standard Model physics, J. High Energy Phys. 10 (2014) 128.

[6] M. B. Einhorn and J. Wudka, The bases of effective field theories, Nucl. Phys. **B876**, 556 (2013).

[7] C. Degrande, N. Greiner, W. Kilian, O. Mattelaer, H. Mebane, T. Stelzer, S. Willenbrock, and C. Zhang, Effective field theory: A modern approach to anomalous couplings, Ann. Phys. (Amsterdam) **335**, 21 (2013).

[8] J. F. Kamenik, J. Shu, and J. Zupan, Review of new physics effects in $t\bar{t}$ production , Eur. Phys. J. C **72**, 2102 (2012).

[9] C. Zhang and S. Willenbrock, Effective-field-theory approach to top-quark production and decay, Phys. Rev. D **83**, 034006 (2011).

[10] B. Grzadkowski, M. Iskrzynski, M. Misiak, and J. Rosiek, Dimension-six terms in the Standard Model lagrangian, J. High Energy Phys. 10 (2010) 085.

[11] W. Buchmuller and D. Wyler, Effective lagrangian analysis of new interactions and flavour conservation, Nucl. Phys. **B268,** 621 (1986).

[12] J. A. Aguilar-Saavedra, A minimal set of top anomalous couplings, Nucl. Phys. **B812,** 181 (2009).

[13] G. Abbiendi *et al.* (OPAL Collaboration), Measurement of alpha(s) with radiative hadronic events, Eur. Phys. J. C **53,** 21 (2008).

[14] Q. H. Cao, B. Yan, J. H. Yu, and C. Zhang, A general analysis of *Wtb* anomalous couplings, arXiv:1504.03785.

[15] K. A. Olive *et al.* (Particle Data Group Collaboration), Review of particle physics, Chin. Phys. C **38,** 090001 (2014).

[16] W. Geng, Report No. FERMILAB-THESIS-2012-46; S. Lee, Report No. FERMILAB-THESIS-2011-07; Y. Sumino, Probe of CP violation in $e^+e^- \to t\bar{t}$ near threshold, arXiv:hep-ph/0007326; D. Atwood, S. Bar-Shalom, G. Eilam, and A. Soni, CP violation in top physics, Phys. Rep. **347,** 1 (2001); A. Brandenburg and J. P. Ma, *CP* odd observables for the top-antitop system produced at $p\bar{p}$ and proton proton colliders, Phys. Lett. B **298,** 211 (1993).

[17] A. O. Bouzas and F. Larios, Probing $tt\gamma$ and ttZ couplings at the LHeC, Phys. Rev. D **88,** 094007 (2013).

[18] F. Hoogeveen, The Standard Model prediction for the electric dipole moment of the electron, Nucl. Phys. **B341,** 322 (1990).

[19] W. Bernreuther, R. Bonciani, T. Gehrmann, R. Heinesch, T. Leineweber, P. Mastrolia, and E. Remiddi, QCD corrections to static heavy quark form-factors, Phys. Rev. Lett. **95,** 261802 (2005).

[20] T. Ibrahim and P. Nath, The top quark electric dipole moment in an MSSM extension with vector like multiplets, Phys. Rev. D **82,** 055001 (2010).

[21] A. Cordero-Cid, J. M. Hernandez, G. Tavares-Velasco, and J. J. Toscano, Bounding the top and bottom electric dipole moments from neutron experimental data, J. Phys. G **35,** 025004 (2008).

[22] U. Baur, A. Juste, L. H. Orr, and D. Rainwater, Probing electroweak top quark couplings at hadron colliders, Phys. Rev. D **71,** 054013 (2005).

[23] A. O. Bouzas and F. Larios, Electromagnetic dipole moments of the top quark, Phys. Rev. D **87,** 074015 (2013).

[24] M. G. Albrow *et al.* (FP420 R and D Collaboration), The FP420 & Project: Higgs and new physics with forward protons at the LHC, JINST **4,** T10001 (2009).

[25] V. Avati and K. Osterberg, Report No. CERN-TOTEM-NOTE–002, 2006.

[26] The CMS and TOTEM Collaborations, Report No. CERN/LHCC 2006-039/G-124.

[27] A. De Roeck, V. A. Khoze, A. D. Martin, R. Orava, and M. G. Ryskin, Ways to detect a light Higgs boson at the LHC, Eur. Phys. J. C **25,** 391 (2002).

[28] D. G. d'Enterria, Forward physics at the LHC, arXiv:0708.0551.

[29] O. Kepka and C. Royon, Anomalous $WW\gamma$ coupling in photon-induced processes using forward detectors at the LHC, Phys. Rev. D **78,** 073005 (2008).

[30] S. C. Inan, Exclusive excited leptons search in two lepton final states at the CERN-LHC, Phys. Rev. D **81,** 115002 (2010).

[31] E. Chapon, C. Royon, and O. Kepka, Anomalous quartic *W W* gamma gamma, *Z Z* gamma gamma, and trilinear WW gamma couplings in two-photon processes at high luminosity at the LHC, Phys. Rev. D **81,** 074003 (2010).

[32] S. Atag and A. A. Billur, Possibility of determining τ lepton electromagnetic moments in $\gamma\gamma \to \tau^+\tau^-$ process at the CERN-LHC, J. High Energy Phys. 11 (2010) 060.

[33] S. C. Inan and A. A. Billur, Polarized top pair production in extra dimension models via photon-photon fusion at the CERN LHC, Phys. Rev. D **84,** 095002 (2011).

[34] A. A. Billur, Anomalous top-gluon couplings in γp collision at the CERN-LHC, Europhys. Lett. **101,** 21001 (2013).

[35] L. N. Epele, H. Fanchiotti, C. A. G. Canal, V. A. Mitsou, and V. Vento, Looking for magnetic monopoles at LHC with diphoton events, Eur. Phys. J. Plus **127,** 60 (2012).

[36] M. Koksal and S. C. Inan, Search for the anomalous interactions of up-type heavy quarks in $\gamma\gamma$ collision at the LHC, Adv. High Energy Phys. **2014,** 315826 (2014).

[37] S. C. Inan, Dimension-six anomalous $tq\gamma$ couplings in $\gamma\gamma$ collision at the LHC, arXiv:1410.3609.

[38] S. Taheri Monfared and S. Fayazbakhsh, Probing anomalous top quark couplings in diffractive events at the LHC, Acta Phys. Pol. B Proc. Suppl. **7,** 579 (2014).

[39] S. Y. Ayazi, H. Hesari, and M. M. Najafabadi, Probing the top quark chromoelectric and chromomagnetic dipole moments in single top *tW*-channel at the LHC, Phys. Lett. B **727,** 199 (2013).

[40] H. Hesari and M. M. Najafabadi, Probing the anomalous couplings of the top quark with gluon at the LHC and Tevatron, Mod. Phys. Lett. A **28,** 1350170 (2013).

[41] A. Senol, $ZZ\gamma$ and $Z\gamma\gamma$ anomalous couplings in γp collision at the LHC, Phys. Rev. D **87,** 073003 (2013).

[42] A. Senol and M. Koksal, Analysis of anomalous quartic $WWZ\gamma$ couplings in γp collision at the LHC, Phys. Lett. B **742,** 143 (2015).

[43] R. Martinez, M. A. Perez, and N. Poveda, Chromomagnetic dipole moment of the top quark revisited, Eur. Phys. J. C **53,** 221 (2008).

[44] S. Heinemeyer, V. A. Khoze, M. G. Ryskin, M. Tasevsky, and G. Weiglein, BSM Higgs physics in the exclusive forward proton mode at the LHC, Eur. Phys. J. C **71,** 1649 (2011).

[45] M. Tasevsky, Exclusive MSSM Higgs production at the LHC after Run I, Eur. Phys. J. C **73,** 2672 (2013).

[46] M. Tasevsky, Review of central exclusive production of the Higgs boson beyond the Standard Model, Int. J. Mod. Phys. A **29,** 1446012 (2014).

[47] M. Tasevsky, Measuring central exclusive processes at LHC, arXiv:0910.5205.

[48] S. Weinberg, Baryon- and Lepton-Nonconserving Processes, Phys. Rev. Lett. **43,** 1566 (1979).

[49] V. M. Budnev, I. F. Ginzburg, G. V. Meledin, and V. G. Serbo, The two-photon particle production mechanism. Physical problems. Applications. Equivalent photon approximation, Phys. Rep. **15,** 181 (1975).

[50] K. Piotrzkowski, Tagging two-photon production at the CERN large hadron collider, Phys. Rev. D **63,** 071502 (2001).

[51] I. Sahin and M. Koksal, Search for electromagnetic properties of the neutrinos at the LHC, J. High Energy Phys. 03 (2011) 100.

[52] G. Baur, K. Hencken, D. Trautmann, S. Sadovsky, and Y. Kharlov, Coherent gamma gamma and gamma-A interactions in very peripheral collisions at relativistic ion colliders, Phys. Rep. **364**, 359 (2002).

[53] H. Sun, Large extra dimension effects through light-by-light scattering at the CERN LHC, Eur. Phys. J. C **74**, 2977 (2014).

[54] V. A. Khoze, A. D. Martin, and M. G. Ryskin, Prospects for new physics observations in diffractive processes at the LHC and Tevatron, Eur. Phys. J. C **23**, 311 (2002).